Proceedings of the 9th International Symposium on
Dynamics and Control of Process Systems (DYCOPS 2010),
Leuven, Belgium, July 5-7, 2010
Mayuresh Kothare, Moses Tade, Alain Vande Wouwer, Ilse Smets (Eds.)

Multiscale modeling and optimization of an atomic layer deposition process for nanomanufacturing applications

Raymond A. Adomaitis

Department of Chemical and Biomolecular Engineering, Institute for Systems Research, University of Maryland, College Park, MD 20742, USA (email: adomaiti@umd.edu)

Abstract: A multiscale model of atomic layer deposition (ALD) inside a nanoporous material is developed in this paper. The overall model couples lattice Monte Carlo simulators describing molecular-scale growth of the ALD film to a continuum description of the precursor transport within the nanopore. The multiscale simulator is used to study how intra-pore precursor depletion leads to nonuniform ALD films and can be used to examine whether film properties, such as composition and surface roughness, are functions of position within the pore. The simulator developed in this study is used to optimize the film growth process by manipulating the precursor species exposure level to produce nearly perfectly uniform films within the nanopores.

Keywords: Multiscale simulation; nanomanufacturing; atomic layer deposition; process optimization

1. INTRODUCTION

Atomic layer deposition (ALD) has been used to modify the geometry of nanostructured materials (6; 9), such as nanoporous membranes that serve as templates for the fabrication of nanoengineered devices (4). The increasing importance of ALD as a thin-film manufacturing technique and recognition that ALD does not always produce perfectly conformal films has motivated recent modeling studies. "First-principles" modeling (7) has mostly been limited to the initial growth of ALD films because of the computational difficulties associated with applying large-scale molecular dynamics techniques to simulate growth of ALD films over multiple cycles. Gas-phase species transport within nanopores has been modeled by molecular dynamics and other sophisticated techniques (3). However, the growth and transport models have only been recently been coupled in a complete multiscale simulation (2) capable of predicting film structure over hundreds of ALD cycles.

1.1 The multiscale nature of the problem

In an earlier paper (1), we describe a detailed lattice Monte Carlo model of ALD alumina growth using trimethylaluminum and water as the precursors, [1] and examine the progression of film growth from a crystalline substrate with a fully hydroxylated initial surface (7). In (2), we built on this molecular-scale model of film growth, incorporating that model in a Knudsen-diffusion based transport model within a high aspect ratio anodic aluminum oxide nanopore, examining the interplay between film growth along the nanopore and the resulting modification to the diffusive transport within the pore. The phenomenological and computational aspects of coupling the microscropic model of film growth to the continuum description of transport within the pore were explored in the cited manuscript. Furthermore, a representative simulation was examined to determine if film properties change as a function of position along the length of the nanopore. In this paper, we continue to extend this line of study, and for the first time, apply the multiscale simulator as a means of optimizing film uniformity within the nanopores.

The full ALD reaction/diffusion system is characterized by two time scales: the slower time-scale t (min to hrs) of film growth and the faster time τ corresponding to surface reactions and the exposure period duration. Likewise, there are two length scales: r (nm) corresponding to the pore radius, compositional variations, and surface roughness, and z (μm) the pore length scale. This splits the model problem neatly into a combination of spatial and temporal scales: the molecular-scale surface reaction model characterized by τ and r, the pore evolution model in which the pore radius measured by r depends on time scale t and length scale z, and the gas-phase transport model, which will be integrated over τ, making it a function of t and z.

2. THE FILM GROWTH MODEL

Al_2O_3 ALD growth proceeds by the two half reactions, the first corresponding to the trimethylaluminum (TMA) exposure in which the TMA binds to the oxygen of a surface hydroxyl group (12) and then reacts releasing a methane molecule:

$$\mathrm{AlOH} + \mathrm{Al(CH_3)_3} \rightarrow \mathrm{Al\text{-}O\text{-}Al(CH_3)_2} + \mathrm{CH_4}.$$

⋆ The author acknowledges the support of the National Science Foundation through grant NSF-CBET 0828410.

[1] Precursors are the gas phase chemical species that react to form the deposited film; see, e.g., (10) for an overview relevant to ALD.

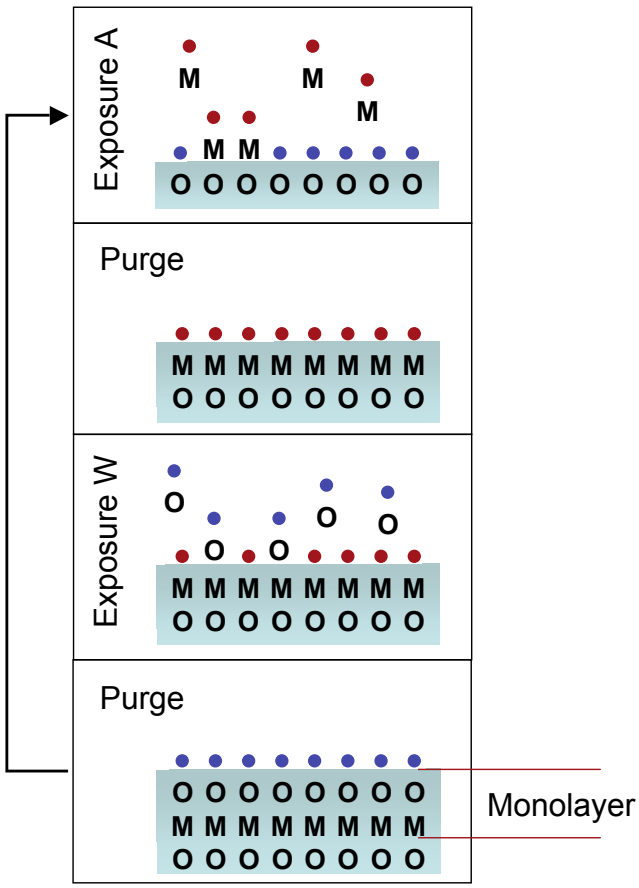

Fig. 1. *An idealized atomic layer deposition (ALD) process, illustrating the two precursor (A, W) exposure and two purge steps making one complete ALD cycle.*

The surface hydroxyl groups are reformed during the subsequent half reaction when water is used as the precursor:

$$\text{Al-O-Al}(\text{CH}_3)_2 + 2\text{H}_2\text{O} \rightarrow \text{Al-O-Al}(\text{OH})_2 + 2\text{CH}_4.$$

An idealized illustration of one complete ALD cycle is shown in Fig. 1, where M· denotes the TMA and O· the water precursor molecules. Of course, the actual reactions are far more complex, and do not normally produce perfect monolayers during each deposition cycle. Numerous studies have examined specific aspects of the ALD reactions; some of these include (5; 7; 10; 12).

To develop a comprehensive model of the atomic layer deposition process, (1) presented a two dimensional lattice to represent the alumina surface as it grows during ALD (see Fig. 2). The rationale behind developing this coarse-grained model of film structure was to provide a simple computational representation of the relative positions of reactive surface groups and film morphology, and not to create a framework for precise representation of the film molecular structure.

The substrate and initial fully hydroxylated growth surface (7) is represented on this lattice, and subsequent reactions with gas phase TMA during the first exposure are simulated using a Monte Carlo approach, taking into account the ability of TMA to react with up to three neighboring

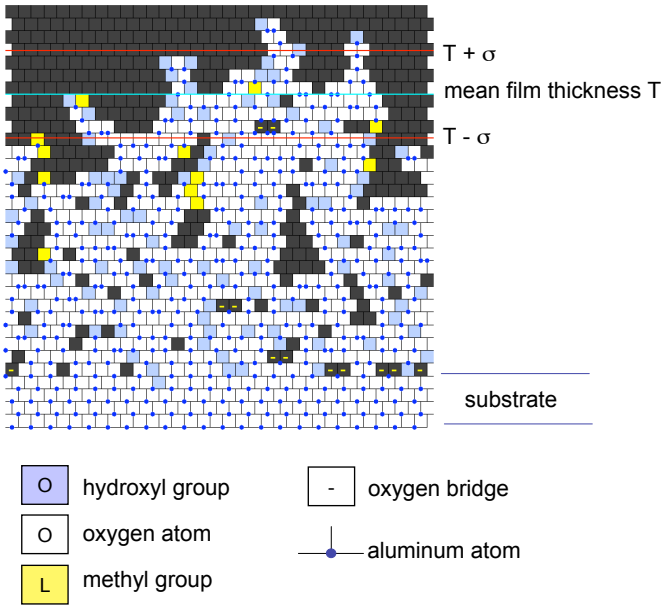

Fig. 2. *Representative ALD film after 50 exposure cycles with $\delta_A = 10$ and $\delta_W = 0.5$ torr sec. This case corresponds to significant water under-exposure.*

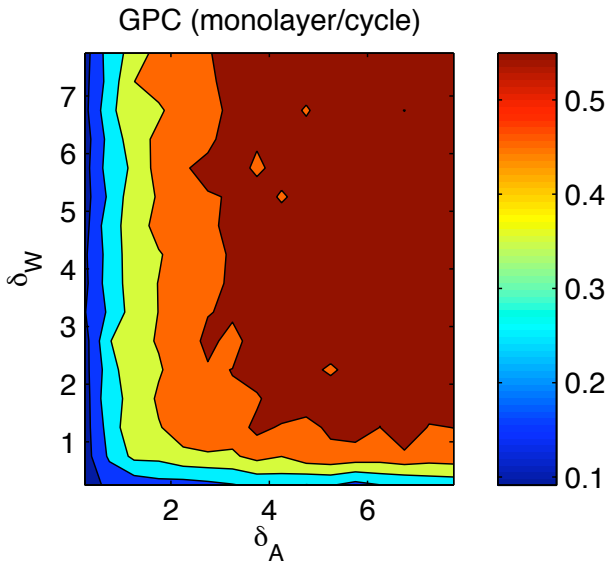

Fig. 3. *Film growth per cycle (GPC) in monolayers/cycle as a function of the two precursor exposure levels δ_A and δ_W. Note the plateau region corresponding to self limited growth at GPC ≈ 0.6 monolayers/cycle.*

surface OH groups. Steric hindrance effects are accounted for by limiting the local surface CH_3 group density, and other reactions also are included in the reaction model (1). Reactions with water are treated in a similar manner. Overall, the MC modeling procedure allows simulation of arbitrarily large numbers of ALD cycles, observing how growth per cycle (GPC), film density ρ, and RMS film surface roughness σ evolve with ALD cycle number and precursor dosages. A representative segment of ALD film is shown in Fig. 2.

Given the precursor partial pressure P_i $(i = A, W)$ during each exposure period, we now define the half-cycle average precursor dose δ_i for TMA and water as

$$\delta_i(z) = \int_0^{\tau_i} P_i(z,\tau)d\tau$$

where τ_i is the length of each exposure period. Using the film growth model, we compute the GPC as a function of the two precursor dosages δ_A, δ_W and plot the results in Fig. 3. This figure maps out the region of self-limited growth, illustrating that for larger values of δ_A and δ_W, no increase in film growth rate occurs. In this region (marked by the darkest red of Fig. 3), the reaction has gone to completion and no further benefit is to be gained by higher precursor exposure levels.

3. PORE TRANSPORT MODELING

Given the relatively low pressure of the ALD process and the small (e.g., 10-100 nm) nanopore diameters, we find Knudsen numbers on the order of 1000, clearly indicating Knudsen diffusion as the precursor transport mode within the pore (3; 11). Based on the pore geometry illustrated in Fig. 4, the following relationship balancing the overall transport and reaction that takes place over each exposure period can be posed:

Net Knudsen diffusion = ALD surface reactions

and then translated into the following modeling equation

$$\frac{1}{L^2}\frac{\partial}{\partial z}\frac{r^2(z,t)}{RT}\mathcal{D}_i\frac{\partial \delta_i}{\partial z} = \int_0^{\tau_i} 2r(z,t)R_i^c(P_i,z)d\tau \qquad (1)$$

for pore length L, reactor temperature T, pore radius r, and pore axial position z. Again, $i = A, W$ indicate the two precursor species. $R_i^c(P_i, z)$ is the instantaneous rate of precursor consumption by the ALD surface reactions, per unit of growth surface area, and the Knudsen diffusion coefficient is defined by

$$\mathcal{D}_i = \frac{2}{3}r(z,t)\sqrt{\frac{8RT}{\pi M_i}}\left[1 - (L)\mathrm{sgn}\left(\frac{\partial \delta_i}{\partial z}\right)\frac{\partial r/\partial z}{L^2 + (\partial r/\partial z)^2}\right]$$

where R is the gas constant and M_i the molecular mass of each of the precursor species. Notice that the right-most term (enclosed in brackets []) accounts for the enhancement/reduction of the Knudsen diffusion that results from gradients in r along the pore length. Omission of this term can lead to negative partial pressure values and numerical instabilities (2). As discussed earlier, note that $r(z,t)$ is used to indicate that pore diameter evolves slowly relative to the length of the exposure cycles τ_i.

We now define the total number Γ_i of precursor molecules that collide and subsequently react with the growth surface as

$$\Gamma_i(\delta_i(z)) = \int_0^{\tau_i} R_i^c(P_i(z,\tau))d\tau,$$

respectively. Having averaged the two precursor mass balance equations over each half-cycle and using the definitions above gives the greatly simplified two-point boundary-value problem:

$$\frac{d}{dz}r^3(z,t)[1-\epsilon(z,t)]\frac{d\delta_i}{dz} - \alpha_i r(z,t)\Gamma_i(\delta_i) = 0 \qquad (2)$$

with

$$\alpha_i = 3L^2\sqrt{\frac{\pi M_i RT}{8}}$$

and

$$\epsilon(z,t) = (L)\mathrm{sgn}\left(\frac{d\delta_i}{dz}\right)\frac{\partial r/\partial z}{L^2 + (\partial r/\partial z)^2}$$

subject to the two pore mouth boundary conditions

$$\delta_i(0) = \delta_i^o \quad \text{and} \quad \delta_i(1) = \delta_i^1.$$

The constants α_i essentially lump the Knudsen diffusion coefficient, the pore aspect ratio, and the geometry factor relating pore gas-phase depletion to the precursor consumption rate by the ALD surface reactions into a single term.

4. MULTISCALE SIMULATION

The final form of the boundary value problem (2) subject to the specified boundary conditions is discretized using an orthogonal polynomial collocation technique, where the polynomials are globally defined over $z \in [0, 1]$. If $\mathbf{A}$ is the discrete (1st order) differentiation array produced using the collocation procedure, the discretized equations are written as

$$\mathbf{A}\,\mathrm{diag}(\mathbf{r^3} \circ [1-\epsilon])\mathbf{A}\delta_\mathbf{i} - \alpha_i \mathbf{r} \circ \Gamma_i(\delta_\mathbf{i}) = \mathbf{0}$$

where $\circ$ is the Hadamard (term-by-term) product and diag() indicates a diagonal array with $\mathbf{r^3} \circ [1-\epsilon]$ as the diagonal elements.

A Newton-Raphson procedure then is used to solve each set discretized equations, first for $\delta_A(z)$ during the TMA exposure step and then $\delta_W(z)$ during the water exposure. We write $\delta_i(z)$ instead of the vector of discretized values $\delta_\mathbf{i}$ because the former is found from the latter by using the orthogonal polynomial sequence and discrete transformation array of the collocation procedure.

A vector of objects defining the *local* film properties is subjected to the Monte Carlo simulation procedure corresponding to the appropriate half reaction exposure level $\delta_i(z_j)$. A film growth model object is defined at every collocation point to determine the GPC and consumption Γ_i of the precursors at each point z_j. To couple the stochastic model of film growth to the deterministic model of precursor transport, by regression we fit a model of the form

$$\Gamma_i = \Gamma_i^\infty\left(1 - e^{a_i\delta_i}\right)$$

where Γ_i^∞ and a_i are the model parameters to be fitted after each half-cycle. We note that the most computationally difficult elements of the Jacobian array necessary for the Newton procedure all lie on the diagonal and correspond to $d\Gamma_i(\delta_i(z_j))/d\delta_i(z_j)$. The more numerous off-diagonal elements correspond to the differentiation array $\mathbf{A}$, which only must be computed at the outset of the simulation.

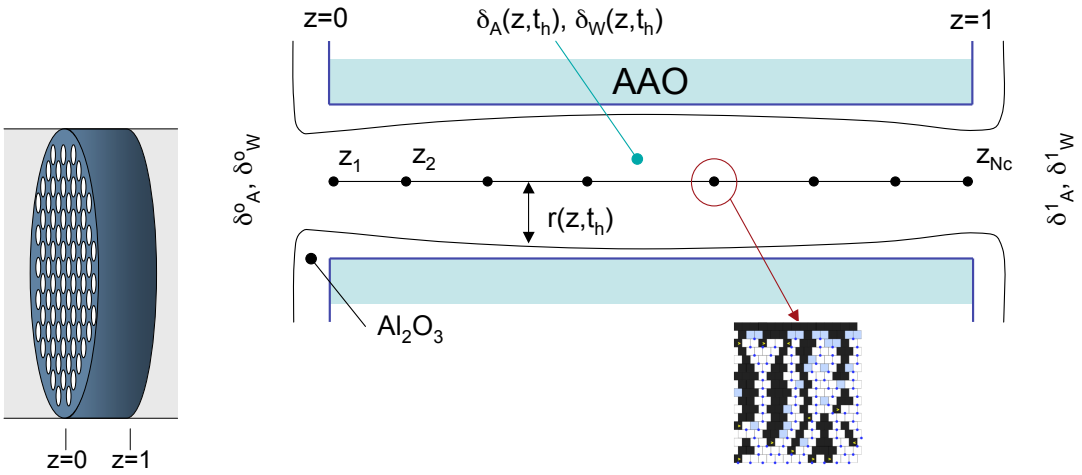

Fig. 4. *Nanoporous film (left) and closeup of an individual pore geometry (right) illustrating the scale z over which which the cycle-averaged TMA and water exposure levels (δ_A and δ_W, respectively) are defined. Individual lattice Monte Carlo film growth models are evaluated at the collocation points z_j.*

Overall, this Jacobian structure is exploited to produce a relatively efficient computing procedure that scales nearly linearly with collocation number N_c.

After convergence of the Newton procedure, the pore radius profile is updated using the local GPC values:

$$r(z_j, t_h) = r(z_j, t_{h-1}) + GPC(z_j, t_{h-1})$$

where h is the cycle number and j the collocation point indices. Using the updated pore radius profile, the following exposure levels δ_i then are computed for the next exposure cycle.

5. REPRESENTATIVE RESULTS

As a representative simulation, we consider a nanoporous membrane that is open at both ends (such as in Fig. 4) subject to the symmetric boundary conditions $\delta_A(0) = \delta_A(1) = 40\,Torr \cdot s$, i.e., a four second exposure to each precursor supplied at a pressure of $10\,Torr$, and $\delta_W(0) = \delta_W(1) = 32\,Torr \cdot s$. These exposure levels are far above those values that are required to saturate the growth surface when no mass transfer resistance is present (see Fig. 3); the motivation for choosing these relatively high values was to increase the transport of precursors to the pore central region. The initial pore diameter was set at $30\,nm$ and pore length to be $3\,\mu m$ resulting in values of $\alpha_A = 10800$ and $\alpha_W = 5400\,Torr\,s\,nm^4/molecule$. The difference between the two coefficients is attributable to the differences in Knudsen diffusion coefficient of the two precursor species at $T = 500\,K$.

Results of this representative simulation are shown in Fig. 5. A total of 85 ALD cycles were simulated, at which the pore mouths have been substantially reduced due to the build up of the ALD film. Early in the ALD deposition process (e.g., 25 cycles, second profile from the top in Fig. 5) little resistance to diffusion within the pores is encountered by either precursor, giving a relatively uniform film. However, as the pore diameter shrinks, resistance to precursor diffusion in the pore mouth region increases, resulting in precursor depletion in the pore central region and reduced growth - the reduced precursor exposure level is denoted by the blue end of the color scale and by the decreasing values of center(δ_A) and center(δ_W) in Fig. 5, right. Once started, this becomes a self-accelerating process, with pore closure occurring relatively rapidly after the onset of the nonuniform deposition.

5.1 Dosage optimization

Given the self-limiting nature of the ALD process and that we have identified the limits of δ_A and δ_W in Fig. 3 above which the maximum deposition rate will take place, we can formulate a relatively simple process optimization procedure in which the boundary values of (2) are adjusted so that the minimum values of $\delta_A(z)$ and $\delta_W(z)$ equal $5\,Torr \cdot s$. The corresponding boundary values, denoted as $bc(\delta_A)$ and $bc(\delta_W)$ in Fig. 6, which were fixed during the ALD cycles described previously, now will increase with cycle number as the pore radius shrinks.

While conceptually straightforward, the computational procedure used to compute the *minimal* boundary values of the exposure levels δ_i necessary to assure deposition uniformity throughout the pore requires a modification of the Newton-Raphson technique described earlier. In this optimization procedure, the variable/parameter status of the exposure boundary and pore centerpoint values are switched. Thus, the new residual equation $\delta_i(z = L/2) - 5 = 0$ replaces the discretized precursor material balance at the pore center, a simple procedure if an odd number of collocation points N_c is used. In this procedure, the boundary δ_i thus are computed directly; the modified discretized problem converges quadratically under the Newton-Raphson procedure and is computationally comparable to the original simulation procedure, retaining its $\mathcal{O}(N_c)$ scaling.

Under the optimized conditions shown in Fig. 6, the minimum (centerpoint) values of each precursor exposure levels remain constant at the setpoint of $5\,Torr \cdot s$. What changes is the dose levels at the pore mouths; both the TMA and water dosages increase with decreasing pore radius, compensating for the increased resistance due to the narrowing pore. While very high exposure levels are

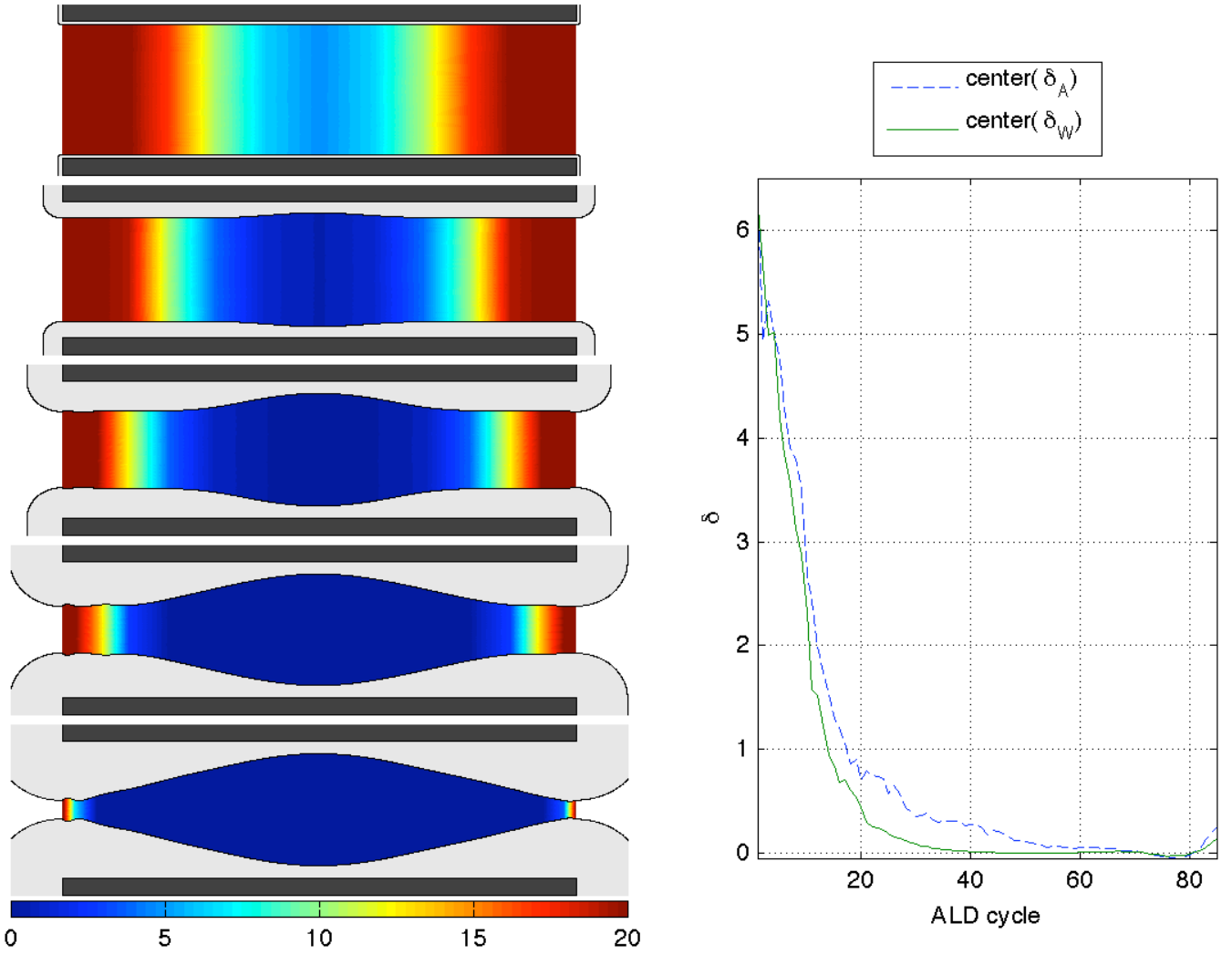

Fig. 5. *Base case simulation showing pore deposition profile snapshots corresponding to cycles 5, 25, 45, 65, and 85 (top to bottom, left). Deposited film is shown in gray, original pore outline in black, along with the gas phase TMA exposure level $\delta_A(z)$. The color bar indicates δ_A in Torr · s. Minimum exposure levels within the pore are shown at right illustrating how the pore central-region exposure levels fall to zero due to depletion within the pore.*

required as the pore radius shrinks to zero, we see that it remains possible to control the pore radius uniformity though all the ALD cycles. Because the area under each curve in the $bc(\delta_i)$ vs. cycle-number plots corresponds to total precursor consumption of this process, further investigation of other modes of ALD operation to decrease precursor utilization is underway to improve the efficiency of precursor utilization.

REFERENCES

[1] Adomaitis, R. A., A lattice Monte Carlo simulation approach for amorphous Al_2O_3 growth in an atomic layer deposition process, *Submitted for publication* (2009).

[2] Adomaitis, R. A., Development of a multiscale model for an atomic layer deposition process, *J. Crystal Growth* **312** 1449-1452 (2010).

[3] Albo, S. E., L. J. Broadbelt, and R. Q. Snurr, Multiscale modeling of transport and residence times in nanostructured membranes. *AIChE J* **52** 3679-3687 (2006).

[4] Banerjee, P., I. Perez, L. Henn-Lecordier, S. B. Lee, and G. W. Rubloff, Nanotubular metal-insulator-metal capacitor arrays for energy storage, *Nature Nanotech.* (2009).

[5] Dillon, A. C., A. W. Ott, J. D. Way, and S. M. George, Surface chemistry of Al_2O_3 using $Al(CH_3)_3$ and H_2O in a binary reaction sequence, *Surf. Sci.* **322** (1995) 230-242.

[6] Elam, J. W., G. Xiong, C. Y. Han, H. H. Wang, J. P. Birrell, U. Welp, J. N. Hryn, M. J. Pellin, T. F. Baumann, J. F. Poco, and J. H. Satcher, Jr., Atomic layer deposition for the conformal coating of nanoporous materials, *J. Nanomaterials* (2006) 1-5.

[7] Elliott, S. D. and J. C. Greer, Simulating the atomic layer deposition of alumina from first principles, *J. Mater. Chem.* (2004) **14** 3246-3250.

[8] Ott, A. W., K. C. McCarthy, J. W. Klaus, J. D. Way, and S. M. George, Atomic layered controlled deposition of Al_2O_3 films using a binary reaction sequence chemistry, *Appl. Surf. Sci.* **107** (1996) 128-136.

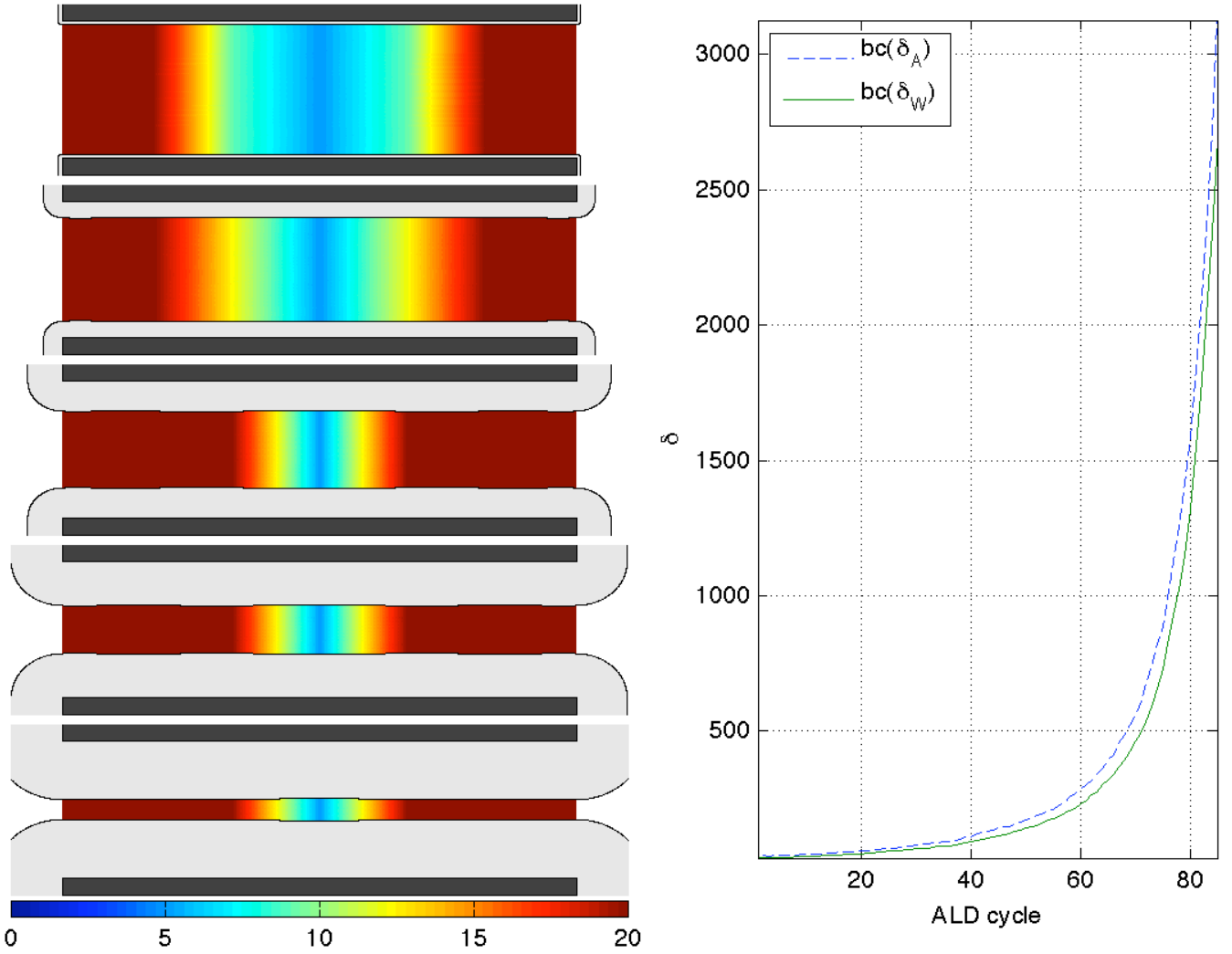

Fig. 6. *Optimized pore deposition profile snapshots corresponding to cycles 5, 25, 45, 65, 85 (top to bottom, left). Deposited film is shown in gray, original pore outline in white, along with the gas phase TMA dosage level* $\delta_A(z)$. *The color bar indicates* δ_A *in* $Torr \cdot s$. *The boundary (maximum) exposure levels within the pore are shown at right illustrating how the minimum precursor exposure levels within the pore are held constant by the optimization procedure while the boundary values increase to compensate for the increasing resistance to precursor transport.*

[9] Pellin, M. J., P. C. Stair, G. Xiong, J. W. Elam, J. Birrell, L. Curtiss, S. M. George, C. Y. Han, L. Iton, H. Kung, M. Kung, and H.-H. Wang, Mesoporous catalytic membranes: Synthetic control of pore size and wall composition *Cat. Lett.* **102** (2005) 127-130.

[10] Puurunen, R. L., Surface chemistry of atomic later deposition: A case study of the trimethylaluminum/water system, *Appl. Phys. Rev.* **97** 121301 (2005).

[11] Song, L., S. Shen, K. S. Tsakalis, P. E. Crouch, and T. S. Cale, Optimal control for increasing throughput in low pressure chemical vapor deposition, *Proc. 35th CDC*, Dec. 1996.

[12] Widjaja, Y. and C. B. Musgrave, Quantum chemical study of the mechanism of aluminum oxide atomic layer deposition. *Appl. Phys. Lett.* **80** 3304-3306 (2002).